Unusual kinetics of thermal decay of dim-light photoreceptors in vertebrate vision

Ying Guo, Sivakumar Sekharan, Jian Liu, Victor S. Batista, John C. Tully[1], and Elsa C. Y. Yan[1]

Department of Chemistry, Yale University, New Haven, CT 06520

Contributed by John C. Tully, June 13, 2014 (sent for review April 5, 2014)

We present measurements of rate constants for thermal-induced reactions of the 11-*cis* retinyl chromophore in vertebrate visual pigment rhodopsin, a process that produces noise and limits the sensitivity of vision in dim light. At temperatures of 52.0–64.6 °C, the rate constants fit well to an Arrhenius straight line with, however, an unexpectedly large activation energy of 114 ± 8 kcal/mol, which is much larger than the 60-kcal/mol photoactivation energy at 500 nm. Moreover, we obtain an unprecedentedly large prefactor of $10^{72\pm5}$ s^{-1}, which is roughly 60 orders of magnitude larger than typical frequencies of molecular motions! At lower temperatures, the measured Arrhenius parameters become more normal: E_a = 22 ± 2 kcal/mol and A_{pref} = $10^{9\pm1}$ s^{-1} in the range of 37.0–44.5 °C. We present a theoretical framework and supporting calculations that attribute this unusual temperature-dependent kinetics of rhodopsin to a lowering of the reaction barrier at higher temperatures due to entropy-driven partial breakup of the rigid hydrogen-bonding network that hinders the reaction at lower temperatures.

non-Arrhenius | dim-light vision | transition state theory | isomerization rate

Rhodopsin is a vertebrate dim-light photoreceptor. Molecular studies of rhodopsin in recent decades have largely focused on its photochemistry and photoactivation (1–3). However, complete understanding of rhodopsin's function requires characterization of its thermal properties because thermal isomerization of the 11-*cis* retinyl chromophore can trigger the same physiological response as photo-isomerization, generating false visual signals as dark noise that jeopardizes photosensitivity (4–6). To enhance dim-light vision, rhodopsin has evolved to acquire remarkable thermal stability with a half-life of 420 y as determined by electrophysiological experiments using the outer segments of rod cells at 36 °C (4). However, the molecular mechanism for the thermal stability has remained unclear. Here, we have addressed this by exploring the temperature dependence of thermal decay rate constants $k(T)$ associated with isomerization of the retinyl chromophore and hydrolysis of the chromophore protonated Schiff-base (PSB) linkage, for temperatures ranging from the physiological temperature of 37.0 °C to 64.6 °C. In the upper range of temperatures from 52.0 °C to 64.6 °C, we find that the rate constants determined by UV-visible spectroscopy follow a linear Arrhenius model, $k(T) = A_{pref} \exp(-E_a/k_BT)$, where k_B is the Boltzmann constant (Fig. 1*A*). The slope, however, is very steep, giving an elevated activation energy, E_a = 114 ± 8 kcal/mol. Surprisingly, this value is much higher than the photoactivation energy at visible wavelengths (60 kcal/mol at 500 nm). E_a is also much higher than the reaction enthalpy change (32–35 kcal/mol) (7, 8) (Fig. 1*B*). In the lower temperature range of our rate constant measurements, 37.0–44.5 °C, the slope of the Arrhenius plot decreases abruptly, as shown in Fig. 1*A*. Fitting a straight line through the low temperature points produces an activation energy E_a = 22 ± 2 kcal/mol, although with only three data points, the precise value must be viewed with caution. In the upper temperature range of our measurements, the Arrhenius prefactor was found to be enormous, $A_{pref} = 10^{72\pm5}$ s^{-1}, which is many orders of magnitude larger than the 10^{12}–10^{15} s^{-1} timescale of molecular motions. In fact, the largest Arrhenius prefactor we have been able to find in the literature for a thermal unimolecular reaction is ~10^{38} s^{-1} (9). By contrast, in the lower temperature range of our measurements, the prefactor was found to have a more typical value, estimated from the three data points to be about $10^{9\pm1}$ s^{-1}. Similar activation energies can be inferred from Arrhenius plots previously obtained by Hubbard in 1958 (~100 kcal/mol) (10) and by Janz and Farrens in 2004 (~103 kcal/mol) (11). However, they did not explicitly report prefactors, and the origins of the large E_a and the sharp bending of the Arrhenius plot remained unexplored. Here, we present a model to describe the molecular origins of the observed rate parameters, including the extraordinarily large prefactor and dramatic inflection in the Arrhenius plot, and discuss the implications of this behavior to rhodopsin's dim-light photoreceptor function. We tackle this puzzling phenomenon by combining the kinetic and thermodynamic analysis with theoretical and molecular modeling. The comparative analysis of the unusual kinetics observed at 52.0–64.6 °C to the more normal Arrhenius behavior observed at lower temperatures (T < 46 °C) provides insights into the potential role of hydrogen bonds (H-bonds) in the reaction mechanism.

Results and Discussion

Fig. 2*A* shows the time-dependent UV-visible spectra of our expressed and purified bovine rhodopsin in 0.1% n-dodecyl-β-D-maltoside (DDM) after being added to a preheated buffer that initiates the thermal decay, as in previous studies (12, 13). The optical density at 500 nm (OD_{500}) decreases, whereas absorption at 380 nm (OD_{380}) increases, due to formation of all-*trans* retinyl

Significance

For vertebrates to have sensitive vision in dim light, any background signals in the dark must be minimal, i.e., thermal reactions of the visual pigment rhodopsin must be very slow. Through discovery of an unprecedented temperature dependence of the thermal reactions of rhodopsin, with associated theoretical modeling, this study has provided a quantitative measure of the contribution to the thermal stability of rhodopsin from the rigid hydrogen bond-stabilized structure of the native protein. These findings may have implications to progressive retinal degenerative eye diseases such as retinitis pigmentosa and to molecular evolution of vertebrate visual pigments. The added stabilization provided by the hydrogen bonding network may prove to be a general feature in a wide variety of proteins.

Author contributions: V.S.B., J.C.T., and E.C.Y.Y. designed research; Y.G., S.S., J.L., V.S.B., J.C.T., and E.C.Y.Y. performed research; S.S. performed theoretical calculations; Y.G. and J.L. performed experiments; Y.G. and E.C.Y.Y. analyzed data; Y.G., S.S., V.S.B., J.C.T., and E.C.Y.Y. wrote the paper.

The authors declare no conflict of interest.

Freely available online through the PNAS open access option.

[1]To whom correspondence may be addressed. Email: john.tully@yale.edu or elsa.yan@yale.edu.

This article contains supporting information online at www.pnas.org/lookup/suppl/doi:10.1073/pnas.1410826111/-/DCSupplemental.

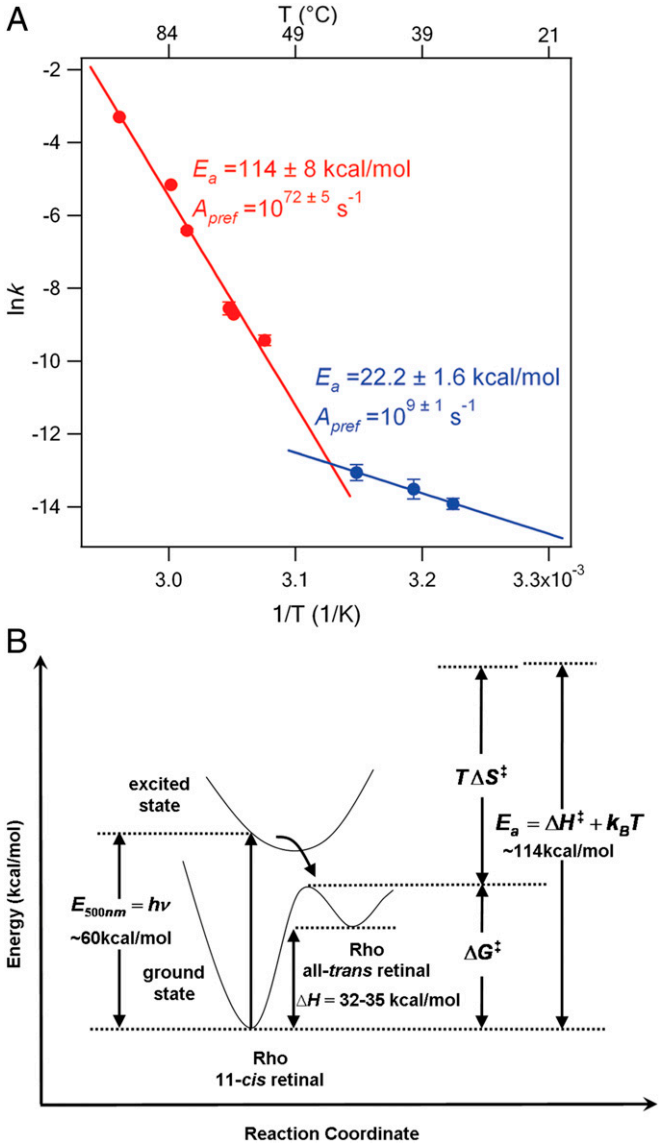

Fig. 1. (*A*) Natural logarithm of our measured rate constants plotted vs. inverse temperature. Error bars represent 1 SD. Straight lines are fitted separately to the lower-temperature (blue dots) and upper-temperature (red dots) regions. (*B*) Schematic of energy surfaces for ground and excited electronic states of rhodopsin and decomposition of Arrhenius activation energy.

chromophore bound at the active site or free retinal in solution in either the all-*trans* or 11-*cis* form. The decay of OD_{500} in the temperature range 52.0–64.6 °C fits a single exponential function, yielding the rate constant of thermal decay (k_{TD}; Fig. 2*B*; *SI Text*). The data in the upper temperature range fit a linear Arrhenius plot (Fig. 2*C*) with $R = 0.9902$, a *y*-intercept of 166.8 ± 12.3, and a slope of $-(5.74 \pm 0.41) \times 10^4$ K^{-1}, yielding $E_a = 114 \pm 8$ kcal/mol and $A_{pref} = 10^{72\pm5}$ s^{-1}. Fig. 2 *E* and *F* shows the Arrhenius plots for thermal isomerization and hydrolysis of the PSB, which are the two competing reactions responsible for thermal decay (12, 13) (Fig. 2*D*). These measurements were carried out only for the more interesting upper temperature region. Both processes also exhibit unusually large E_a and A_{pref} (Fig. 2 *E* and *F*). The decay of OD_{500} in the lower temperature range of our measurements, 37.0–44.5 °C also exhibits approximate straight-line Arrhenius kinetics (Fig. 1*A*), but with dramatically different slope and prefactor: $E_a \sim 22$ kcal/mol and $A_{pref} \sim 4 \times 10^9$ s^{-1}. Above 64.6 °C, including the melting temperature, the 500-nm peak disappears and shifts to 380 nm within a second. Thus, the rates are too fast (<1 s) to be measured by our method.

A key to understanding the origin of the elevated E_a in the upper temperature range is to recognize that E_a is not the free energy difference, $\Delta G^{\ddagger}$, but rather is related to the enthalpy of formation, $\Delta H^{\ddagger}$, of the transition state from the reactant state (14), as shown by transition state theory (TST)

$$k = \frac{k_BT}{h}\exp\left[\frac{-\Delta G^{\ddagger}}{k_BT}\right] = \frac{k_BT}{h}\exp\left[\frac{\Delta S^{\ddagger}}{k_B}\right]\exp\left[\frac{-\Delta H^{\ddagger}}{k_BT}\right], \quad [1]$$

where k is the rate constant and h is Planck's constant. The activation enthalpy $\Delta H^{\ddagger}$, free energy $\Delta G^{\ddagger}$, and entropy $\Delta S^{\ddagger}$ correspond to the thermodynamic quantities for the system when constrained to the transition state relative to the reactant state and can depend on temperature. E_a is the slope of the Arrhenius plot and is constant in a linear regime about $T = T_0$

$$E_a = -k_B\frac{\partial \ln k}{\partial(1/T)}\bigg|_{T=T_0} = \Delta H_0^{\ddagger} + k_BT_0, \quad [2]$$

Fig. 1*A* shows that ln k vs. $1/T$ is approximately linear, but with different slopes in the two different temperature ranges of our measurements (37.0 °C < T < 44.5 °C and 52.0 °C < T < 64.6 °C), giving vastly different enthalpies of activation of 22 and 114 kcal/mol. TST relates the Arrhenius prefactor A_{pref} to the entropy of activation $\Delta S^{\ddagger}$

$$\Delta S_0^{\ddagger} = k_B \ln\left(hA_{pref}/k_BT_0\right) - k_B. \quad [3]$$

For the lower temperature range, using our experimentally determined $E_a = 22$ kcal/mol and $A_{pref} = 10^9$ s^{-1}, at $T_0 = 41$ °C (the midpoint of the lower experimental range), we obtain the following from Eqs. **1–3**: $\Delta H^{\ddagger} = 21$ kcal/mol, $\Delta S^{\ddagger} = -19$ eu (=−0.019 kcal/mol-K), and $\Delta G^{\ddagger} = 28$ kcal/mol. These values are unsurprising, with negative entropy possibly arising from increased crowding at the transition state during isomerization. Note that, by comparison, for free 11-*cis* retinal in solution, $\Delta S \sim -10$ eu (10). It is worthwhile to point out that both $\Delta H^{\ddagger}$ and $\Delta G^{\ddagger}$ are lower than the energy storage in the primary photoproduct, bathorhodopsin, measured as 35 kcal/mol (7). Whether this suggests thermal activation and photoactivation follow different pathways remains to be further explored. By contrast, for the upper temperature region using our experimentally determined $E_a = 114$ kcal/mol and $A_{pref} = 10^{72}$ s^{-1}, at $T_0 = 58$ °C (the midpoint of the upper experimental range), we obtain the following from Eqs. **1–3**: $\Delta H^{\ddagger} = 113$ kcal/mol, $\Delta S^{\ddagger} = 269$ eu, and $\Delta G^{\ddagger} = 24$ kcal/mol. Thus, $\Delta G^{\ddagger}$ is still of normal magnitude and, as expected, lower than the photoactivation energy (~60 kcal/mol) (Fig. 1*B*). Of critical significance is $\Delta S^{\ddagger} = 269$ eu, which is of opposite sign and 30 times larger in magnitude than the activation entropy for isomerization of retinal and larger than the molar entropy of melting ice (5.26 eu) by 50 times! An entropy change of this magnitude can only arise from a collective transformation involving many intermolecular interactions. At T_0 = 58 °C, $T\Delta S^{\ddagger} \sim 89$ kcal/mol, thereby driving the reaction by largely compensating the high $\Delta H^{\ddagger} = 113$ kcal/mol. This behavior can be viewed as an example of the well-known "compensation effect" in chemical kinetics in which the activation energy and prefactor of a reaction both change relatively abruptly in the same direction (i.e., compensate), whereas the overall reaction rate changes smoothly. In the case of desorption from a surface, this behavior has sometimes been traced to a phase transition in the substrate or adsorbate layer (15). The magnitudes of the changes in the current example, however, dwarf those of any prior report of

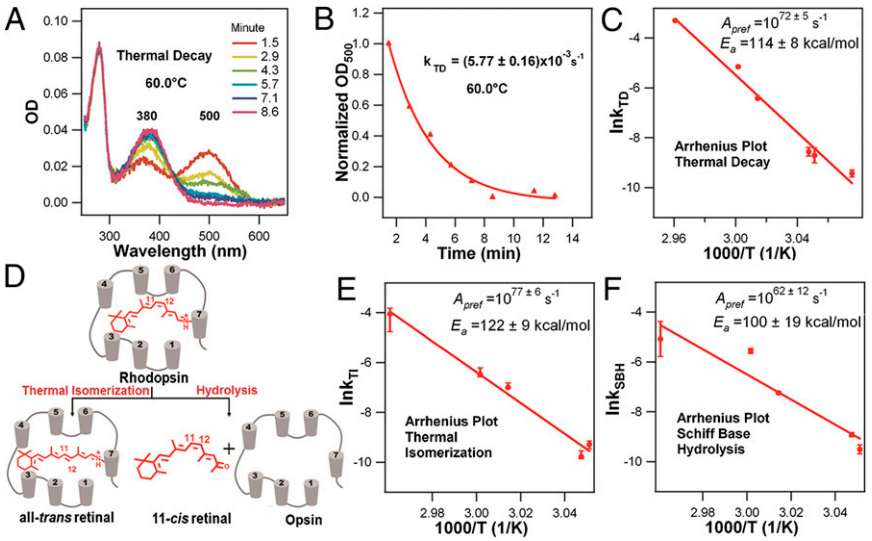

Fig. 2. Thermal reactions of rhodopsin. (*A*) Time-dependent UV-visible spectra of rhodopsin at 60.0 °C. (*B*) Normalized OD_{500} plotted as a function of time and fitted to a single exponential function. (*C*) The Arrhenius plot for k_{TD} in the upper temperature region. (*D*) Two reactions involved in the thermal decay of rhodopsin: isomerization and hydrolysis. The Arrhenius plots in the upper-temperature region for (*E*) thermal isomerization (k_{TI}) and (*F*) Schiff base hydrolysis (k_{SBH}). Buffer condition: 50 mM phosphate buffer (pH 6.5) and 0.1% DDM (error bars represent the SD).

a compensation effect of which we are aware. The observed change in slope of the Arrhenius plot is quite abrupt. A first-order phase transition will produce an inflection point, i.e., a discontinuity in slope (15). Although a finite-sized protein cannot exhibit a true first-order transition, the sharpness of the change-over between the two temperature regimes adds further support to the supposition that a global transformation such as melting or partial melting underlies the observations.

The hypothesis that the extraordinarily large $\Delta S^{\ddagger}$ is indicative of a collective transformation motivated us to investigate the melting of rhodopsin under our experimental conditions. We used circular dichroism spectroscopy to monitor the ellipticity at 222 nm (θ_{222nm}) while the temperature was scanned from 40 °C to 80 °C at a rate of 90 °C/h (*SI Text*). Because negative θ_{222nm} indicates the presence of α-helices, the increase in θ_{222nm} suggests a loss of α-helical structure. In the 65–80 °C range, θ_{222nm} increases abruptly (Fig. 3), reflecting a phase transition at a melting temperature (T_m) 70.8 ± 0.6 °C, consistent with previous

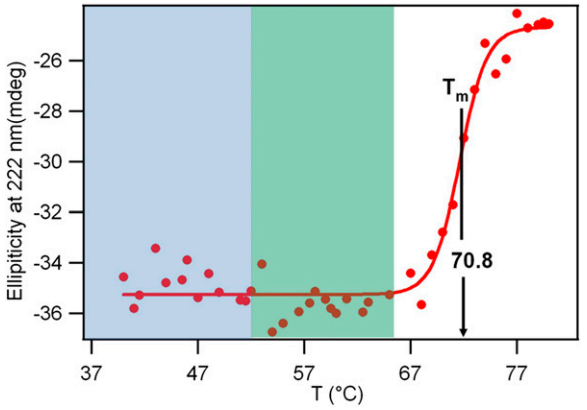

Fig. 3. The melting of rhodopsin. Ellipticity θ_{222nm} monitored as temperature is scanned at a rate of 90 °C/h, yielding the melting temperature to be 70.8 ± 0.6 °C. The experimental lower temperature region is indicated as the blue box, and the upper-temperature region is indicated as the green box ($n \geq 3$; error represents the SD).

reports (16). Analyzing the melting curve using the Van't Hoff equation (*SI Text*), we obtained the molar enthalpy and entropy of melting, H_m = 170 kcal/mol and S_m = 496 eu. Both values are somewhat larger than, but of the same order of magnitude as, the activation enthalpy (113 kcal/mol) and entropy (269 eu) of thermal decay, suggesting that the thermal decay at 52.0–64.6 °C might involve a collective structural transformation related to melting or partial melting.

Structural studies of rhodopsin have revealed dozens of water molecules in the transmembrane domain (Fig. 4*A*), participating in an extended network of ∼100 H-bonds (2, 17). This network is thought to stabilize rhodopsin (2, 18, 19) and suppress thermal isomerization, conferring rhodopsin with extraordinary thermal stability to lower the dark noise and enhance photosensitivity. This hypothesis is supported by the observation that the rates of thermal reactions are slowed down threefold in deuterated water, consistent with a rate-determining step involving water interactions (20). In addition, the mutant S186A where the H-bonds in the retinyl binding site are disrupted (Fig. 4*A*) has rates increased by one to two orders of magnitude (11, 13). It is, therefore, natural to consider that thermal decay at 52.0–64.6 °C, close to T_m, might involve breaking or at least weakening H-bonds associated with internal water molecules. This weakening of H-bonds requires energy, thereby increasing $\Delta H^{\ddagger}$, which must be compensated by a significant increase in internal disorder $\Delta S^{\ddagger}$.

To address the hypothesis that breaking of internal H-bonds can account for the enthalpy and entropy changes observed by kinetic measurements, we compared the 11-*cis*/*trans* isomerization energy barriers in density functional theory quantum mechanics/molecular mechanics (QM/MM) structural models of rhodopsin, assuming various degrees of disruption of internal H-bonds in the transition state (TS). We studied three models, one where the H-bonding network of the initial minimum energy configuration remains intact, one where the H-bonds of internal water molecules at the active site are disrupted in the TS, and a third where the H-bonds of all internal water molecules are randomized at the TS. These QM/MM models were built according to the X-ray structure of bovine rhodopsin (1U19) (17), as described in the *SI Text* (21), using the two-layer ONIOM (our own n-layered integrated molecular orbital and molecular mechanics) scheme, which has been previously used

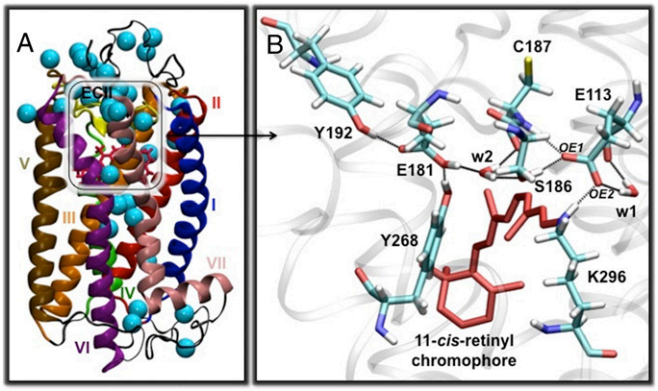

Fig. 4. Computational results. (*A*) The rhodopsin model containing 37 water molecules. (*B*) H-bonding network in the EII loop involving Y268, Y192, E181, S186, C187, E113, and two water molecules (w1 and w2).

for studying related retinal proteins (21–27). The isomerization energy, i.e., the energy of the TS when all H-bonds are intact, was calculated to be 40 kcal/mol, which increases to 106 kcal/mol on disrupting the H-bonds in the TS. These H-bonds involve those of the extracellular loop II (EII loop) in close contact with the retinyl chromophore (Fig. 4*B*) and are mediated by water molecules w1 and w2 and amino acid residues E181, E113, Y192, Y268, S186, and C187 in the active site. The 106 kcal/mol can be partitioned into 78 kcal/mol to break the H-bonds plus 28 kcal/mol to reach the *cis*/*trans* isomerization barrier. Similarly, the isomerization barrier calculated when all internal water molecules are randomized is again 28 kcal/mol. Thus, the isomerization barrier when H-bonds are disrupted is computed to decrease by 12 kcal/mol compared with the barrier when H-bonds are intact. This decrease in the energy barrier supports previous arguments that the H-bonding network stabilizes rhodopsin and suppresses thermal reactions.

We describe our model with reference to the free energy landscape (Fig. 5*A*) and consideration of three temperature regions: (*i*) $T < T_c$, (*ii*) $T_c < T < T_m$, and (*iii*) $T > T_m$, where T_c is the temperature at which partial melting (i.e., disruption of H-bonds) in the transition state becomes significant. As for the QM/MM analysis, we divide $\Delta G^{\ddagger}$ into two parts (Fig. 5*B*): (*i*) breaking of H-bonds in the protein environment ($\Delta G_1^{\ddagger}$) and (*ii*) the barrier for *cis*-to-*trans* isomerization of the retinyl chromophore ($\Delta G_2^{\ddagger}$). We emphasize that the partitioning into these two parts is for convenience in computing thermodynamic state functions and does not imply a two-step reaction mechanism. We express each activation free energy in terms of enthalpy and entropy

$$\Delta G^{\ddagger} = \Delta G_1^{\ddagger} + \Delta G_2^{\ddagger} = \left(\Delta H_1^{\ddagger} - T\Delta S_1^{\ddagger}\right) + \left(\Delta H_2^{\ddagger} - T\Delta S_2^{\ddagger}\right). \quad [4]$$

Using this, we examine how disordering of H-bonds contributes to the activation $\Delta H^{\ddagger}$, $\Delta S^{\ddagger}$, and $\Delta G^{\ddagger}$ in the three temperature regions.

At low temperatures, $T < T_c$, H-bonds remain ordered in both the reactant and transition states, so that $\Delta H_1^{\ddagger} \approx 0$ and $\Delta S_1^{\ddagger} \approx 0$; thus, $\Delta G^{\ddagger} \approx \Delta G_2^{\ddagger}$. The activation entropy, contributed by isomerization, $\Delta S^{\ddagger} \approx \Delta S_2^{\ddagger}$, is therefore of typically small magnitude (negative according to our lower-temperature region measurements). Thus, the system is mainly trapped at the bottom of the energy wells (Fig. 5*F*, green balls) in both the reactant and transition states. The reaction tends to follow the low-temperature path (Fig. 5, blue arrows), E_a and A_{pref} are of normal values for typical chemical reactions, and the free energy of activation $\Delta G^{\ddagger} \sim 28$ kcal/mol. These results agree with Janz and Farrens's kinetic data of thermal decay of rhodopsin (11) (Fig. 5*G*, blue triangles) at temperatures of 37–45 °C, from which we estimate $\Delta G^{\ddagger}$ to be 26 kcal/mol.

At intermediate temperatures, $T_c < T < T_m$, including our upper-temperature experimental range (52.0–64.6 °C), disordering or partial melting of H-bonds starts. Thus, the energy needed to break H-bonds ($\Delta H_1^{\ddagger}$) contributes to the activation enthalpy $\Delta H^{\ddagger} = \Delta H_1^{\ddagger} + \Delta H_2^{\ddagger} = E_a - k_B T$. Hence, E_a is large, measured to be 114 kcal/mol. As indicated by the green balls and arrows of Fig. 5*E*, the system is spread over many configurations at the transition state but is mostly confined to the bottom of the energy well at the reactant state. This difference in entropy between the transition and reactant states yields the large $\Delta S_1^{\ddagger} =$ 269 eu, causing an enormous A_{pref}, as we report, 10^{72} s^{-1}. The Arrhenius plot from our results (Fig. 5*G*, red and blue dots) yields $\Delta G^{\ddagger} \sim 24$ kcal/mol and intersects with the one in the lower-temperature region (blue line) at $T_c = 46.6$ °C.

At $T > T_m$, both reactant and transition states are melted, so there is little change in entropy or enthalpy of activation due to the disordering, i.e., $\Delta H_1^{\ddagger} \approx 0$ and $\Delta S_1^{\ddagger} \approx 0$. Thus, the system at both the reactant and transition states is almost equally spread out along the energy surface (Fig. 5*D*), such that the reaction follows the high-temperature paths (Fig. 5, red arrows). The activation free energy, enthalpy, and entropy are dominated by isomerization, i.e., $\Delta G^{\ddagger} \approx \Delta G_2^{\ddagger}$, $\Delta H^{\ddagger} \approx \Delta H_2^{\ddagger} = E_a - k_B T$, and $\Delta S^{\ddagger} \approx \Delta S_2^{\ddagger}$, giving normal values for all, with $A_{pref} \sim k_B T/h$. Assuming a prefactor of 10^{13} s^{-1}, we use a half time of 7 min for isomerization of 11-*cis* retinyl PSB measured by Rando and Lukton (28) at 25 °C to extrapolate the rate to higher temperatures, which yields an Arrhenius plot (Fig. 5*G*, blue solid line) with a barrier $\Delta G^{\ddagger} = 20$ kcal/mol that intersects the one in the upper experimental temperature range at 67.3 °C, close to T_m. Changing A_{pref} by two orders of magnitude to 10^{11} or 10^{15} s^{-1} (Fig. 5*G*, gray dotted lines) shifts the intersection temperature only by ∼1.5 °C.

The above analysis shows that the reaction barriers $\Delta G^{\ddagger}$ extracted from experiments decrease from 28 to 20 kcal/mol as the temperature increases. This trend supports the following molecular picture: at temperatures considerably below T_m (i.e., $T < T_c$), including the physiological 37 °C, the H-bonding network remains mostly intact ensuring thermal stability by a relatively high activation free energy barrier $\Delta G^{\ddagger}$. At high temperatures $T > T_m$, we propose that $\Delta G^{\ddagger}$ is lower because protein melting leaves the 11-*cis* retinyl chromophore with less steric constraints. At intermediate temperatures ($T_c < T < T_m$), including the upper temperature range of our experiments, 52.0–64.6 °C, the free energy barrier $\Delta G^{\ddagger}$ decreases even though both $\Delta H^{\ddagger}$ and $\Delta S^{\ddagger}$ increase due to the disordering of H-bonds in the TS. In fact, as T approaches T_m, the enthalpic ($\Delta H_1^{\ddagger}$) and entropic terms ($T\Delta S_1^{\ddagger}$) of partial melting start offsetting each other, i.e., $\Delta G_1^{\ddagger} = \Delta H_1^{\ddagger} - T\Delta S_1^{\ddagger} \to 0$, leading to a normal value of $\Delta G^{\ddagger}$. Such a normal value of energy barrier explains why we could observe the thermal reactions in an attainable time scale of seconds to hours at 52.0–64.6 °C, despite an Arrhenius E_a as high as ∼114 kcal/mol.

Our reported findings on thermal decay suggest a potentially important role of the internal H-bonding networks in rhodopsin to the molecular mechanism of dim-light vision, central to retinal-related diseases and molecular evolution in vertebrate visual pigments. We conclude that H-bonds are essential to limit thermal isomerization of the chromophore, thereby increasing the dim-light sensitivity of photoreceptors under physiological temperatures. Mutations that perturb the H-bonding network are therefore expected to increase the dark-noise level. In fact, some of the >100 point mutations identified to cause retinitis pigmentosa (29) are expected to break H-bonds and have been shown to increase the thermal isomerization rate, likely associated with the early symptom of night blindness (30). Because the rod pigment rhodopsin diverged from the cone pigments (31), we propose that rhodopsin might have gained dim-light photosensitivity

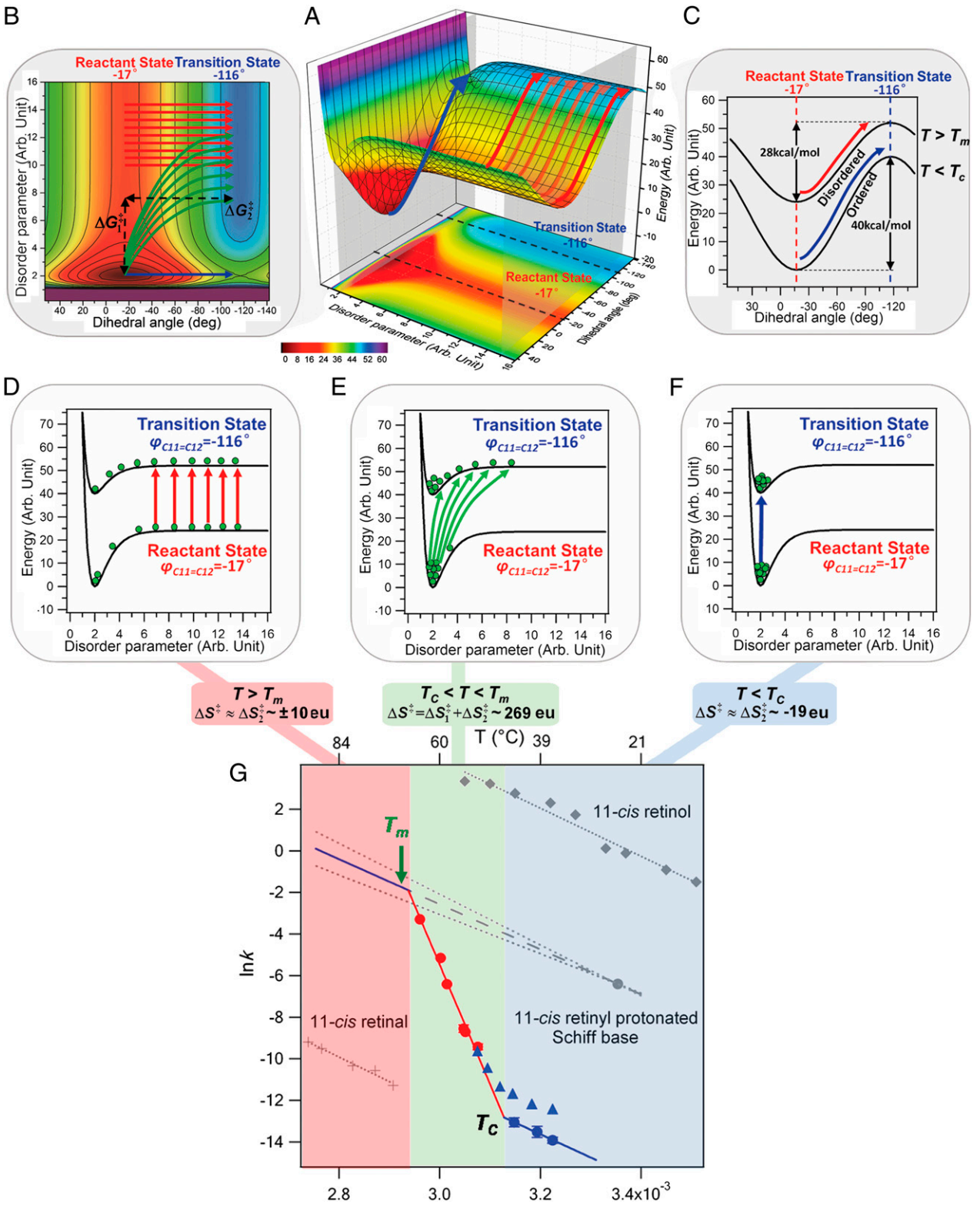

Fig. 5. (*A*) Schematic energy surface. Energy is plotted vs. the disordering parameter (the degree of disordering of H-bonds) and the dihedral angle between the C_{11}–C_{12} double bond (−17° is the reactant state, and −116° is the transition state from the QM/MM calculation as shown in *SI Text*). (*B*) Energy contour plot and the two steps for calculating: disordering of H-bonds ($\Delta G_1^{\ddagger}$) and isomerization of 11-*cis* retinyl chromophore ($\Delta G_2^{\ddagger}$). (*C*) Energy curves corresponding to the two intersection planes in the energy plots for the path at low temperature (blue arrows) with higher, and the path at high temperature (red arrows) with lower. Boltzmann distribution (green balls) at the reactant and transition states for (*D*) $T > T_m$ with ~±10 eu following the red paths, (*E*) $T_C < T < T_m$ with ~269 eu following the numerous green paths, and (*F*) $T < T_C$ with ~−19 eu following the blue path. (*G*) Arrhenius plots spanning three temperature regions, including kinetic data obtained by Janz and Farrnes (11) (blue triangles), in our experiments (red and blue dots), the isomerization of 11-*cis* retinal (33) (gray cross), 11-*cis* retinol (34) (gray diamonds), and 11-*cis* retinyl PSB (28) (gray dots) ($n \geq 3$; error bars represent the SD).

by forming an extensive H-bonding network involving water molecules, which due to their unique mobility could play a distinct functional role in steering the molecular evolution of visual pigments.

Methods

The procedures of preparing rhodopsin were described in detail elsewhere (13). The stable cell line of HEK293S expressing WT bovine opsin was made as previously described (32). The stable cell line was induced with tetracycline and sodium butyrate for expression. The cells were harvested 48 h after induction and regenerated with 11-*cis* retinal (acquired from National Eye Institute, National Institutes of Health) at 5 μM for 4 h at 4.0 °C in the dark. To purify rhodopsin, the regenerated cells were solubilized with 1% (wt/vol) DDM for 4 h at 4.0 °C and purified by an immunobinding method using resins coupled to the 1D4 antibody. The resins were washed three times with 50 mM Tris (pH 6.8), 100 mM NaCl, and 0.1% DDM and another three times with 50 mM sodium phosphate (pH 6.5) and 0.1% DDM (buffer A). The rhodopsin samples were eluted in buffer A containing the 1D5 peptide and then concentrated to ∼20 μM for the experiments. Expanded methods may be found in *SI Text*.

ACKNOWLEDGMENTS. E.C.Y.Y. acknowledges support from National Science Foundation Career Grant MCB-0955407. J.C.T. acknowledges support from Department of Energy, Basic Energy Sciences Grant DE-FG02-05ER15677. V.S.B. acknowledges financial support from National Science Foundation Grant CHE 0911520 and supercomputer time from the National Energy Research Scientific Computing Center and the High Performance Computing facilities at Yale University. J.L. is the recipient of the Anderson Postdoctoral Fellowship.

1. Okada T, Ernst OP, Palczewski K, Hofmann KP (2001) Activation of rhodopsin: New insights from structural and biochemical studies. *Trends Biochem Sci* 26(5):318–324.
2. Li J, Edwards PC, Burghammer M, Villa C, Schertler GF (2004) Structure of bovine rhodopsin in a trigonal crystal form. *J Mol Biol* 343(5):1409–1438.
3. Menon ST, Han M, Sakmar TP (2001) Rhodopsin: Structural basis of molecular physiology. *Physiol Rev* 81(4):1659–1688.
4. Baylor DA, Nunn BJ, Schnapf JL (1984) The photocurrent, noise and spectral sensitivity of rods of the monkey Macaca fascicularis. *J Physiol* 357(Dec):575–607.
5. Baylor DA, Matthews G, Yau KW (1980) Two components of electrical dark noise in toad retinal rod outer segments. *J Physiol* 309(Dec):591–621.
6. Barlow RB, Birge RR, Kaplan E, Tallent JR (1993) On the molecular origin of photoreceptor noise. *Nature* 366(6450):64–66.
7. Cooper A (1979) Energy uptake in the first step of visual excitation. *Nature* 282(5738):531–533.
8. Gascon JA, Batista VS (2004) QM/MM study of energy storage and molecular rearrangements due to the primary event in vision. *Biophys J* 87(5):2931–2941.
9. Liu J, Conboy JC (2005) 1,2-diacyl-phosphatidylcholine flip-flop measured directly by sum-frequency vibrational spectroscopy. *Biophys J* 89(4):2522–2532.
10. Hubbard R (1958) The thermal stability of rhodopsin and opsin. *J Gen Physiol* 42(2):259–280.
11. Janz JM, Farrens DL (2004) Role of the retinal hydrogen bond network in rhodopsin Schiff base stability and hydrolysis. *J Biol Chem* 279(53):55886–55894.
12. Liu J, Liu MY, Fu L, Zhu GA, Yan EC (2011) Chemical kinetic analysis of thermal decay of rhodopsin reveals unusual energetics of thermal isomerization and hydrolysis of Schiff base. *J Biol Chem* 286(44):38408–38416.
13. Liu J, et al. (2011) Thermal properties of rhodopsin: Insight into the molecular mechanism of dim-light vision. *J Biol Chem* 286(31):27622–27629.
14. Steinfeld JI, Francisco JS, Hase WL (1999) *Chemical Kinetics and Dynamics* (Prentice Hall, Upper Saddle River, NJ), 2nd Ed.
15. Estrup PJ, Greene EF, Cardillo MJ, Tully JC (1986) Influence of surface phase-transitions on desorption-kinetics: The compensation effect. *J Phys Chem-Us* 90(17):4099–4104.
16. Khan SMA, Bolen W, Hargrave PA, Santoro MM, McDowell JH (1991) Differential scanning calorimetry of bovine rhodopsin in rod-outer-segment disk membranes. *Eur J Biochem* 200(1):53–59.
17. Okada T, et al. (2004) The retinal conformation and its environment in rhodopsin in light of a new 2.2 A crystal structure. *J Mol Biol* 342(2):571–583.
18. Okada T, et al. (2002) Functional role of internal water molecules in rhodopsin revealed by X-ray crystallography. *Proc Natl Acad Sci USA* 99(9):5982–5987.
19. Angel TE, Gupta S, Jastrzebska B, Palczewski K, Chance MR (2009) Structural waters define a functional channel mediating activation of the GPCR, rhodopsin. *Proc Natl Acad Sci USA* 106(34):14367–14372.
20. Liu J, et al. (2009) Thermal decay of rhodopsin: Role of hydrogen bonds in thermal isomerization of 11-cis retinal in the binding site and hydrolysis of protonated Schiff base. *J Am Chem Soc* 131(25):8750–8751.
21. Sekharan S, Morokuma K (2011) QM/MM study of the structure, energy storage, and origin of the bathochromic shift in vertebrate and invertebrate bathorhodopsins. *J Am Chem Soc* 133(13):4734–4737.
22. Sekharan S, Altun A, Morokuma K (2010) QM/MM study of dehydro and dihydro β-ionone retinal analogues in squid and bovine rhodopsins: Implications for vision in salamander rhodopsin. *J Am Chem Soc* 132(45):15856–15859.
23. Sekharan S, Morokuma K (2011) Why 11-cis-retinal? Why not 7-cis-, 9-cis-, or 13-cis-retinal in the eye? *J Am Chem Soc* 133(47):19052–19055.
24. Sekharan S, Katayama K, Kandori H, Morokuma K (2012) Color vision: "OH-site" rule for seeing red and green. *J Am Chem Soc* 134(25):10706–10712.
25. Sekharan S, et al. (2013) Spectral tuning of ultraviolet cone pigments: An interhelical lock mechanism. *J Am Chem Soc* 135(51):19064–19067.
26. Sekharan S, Wei JN, Batista VS (2012) The active site of melanopsin: The biological clock photoreceptor. *J Am Chem Soc* 134(48):19536–19539.
27. Pal R, Sekharan S, Batista VS (2013) Spectral tuning in halorhodopsin: The chloride pump photoreceptor. *J Am Chem Soc* 135(26):9624–9627.
28. Lukton D, Rando RR (1984) On the amine-catalyzed isomerization of vitamin-a aldehydes. *J Am Chem Soc* 106(1):258–259.
29. Hartong DT, Berson EL, Dryja TP (2006) Retinitis pigmentosa. *Lancet* 368(9549):1795–1809.
30. Liu MY, et al. (2013) Thermal stability of rhodopsin and progression of retinitis pigmentosa: Comparison of S186W and D190N rhodopsin mutants. *J Biol Chem* 288(24):17698–17712.
31. Yokoyama S (2000) Molecular evolution of vertebrate visual pigments. *Prog Retin Eye Res* 19(4):385–419.
32. Yan ECY, et al. (2007) Photointermediates of the rhodopsin S186A mutant as a probe of the hydrogen-bond network in the chromophore pocket and the mechanism of counterion switch. *J Phys Chem C* 111(25):8843–8848.
33. Hubbard R (1966) The stereoisomerization of 11-cis-retinal. *J Biol Chem* 241(8):1814–1818.
34. McBee JK, Van Hooser JP, Jang F, Palczewski K (2001) Isomerization of 11-cis-retinoids to all-trans-retinoids in vitro and in vivo. *J Biol Chem* 276(51):48483–48493.